ACS APPLIED MATERIALS & INTERFACES

www.acsami.org

Research Article

Novel Method for Fabricating Visible-Light Phototransistors Based on a Homojunction-Porous IGZO Thin Film Using Mechano-Chemical Treatment

I. Sak Lee,[§] Joohye Jung,[§] Dong Hyun Choi, Sujin Jung, Kyungmoon Kwak, and Hyun Jae Kim*

Cite This: *ACS Appl. Mater. Interfaces* 2021, 13, 35981−35989

Read Online

ACCESS | Metrics & More | Article Recommendations | Supporting Information

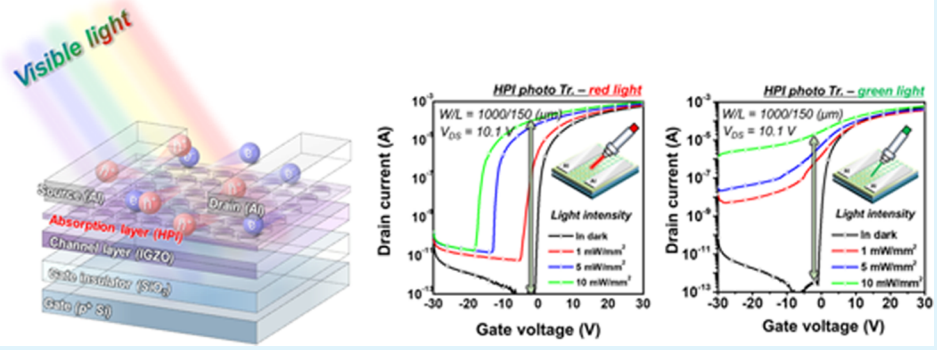

ABSTRACT: A homojunction-structured oxide phototransistor based on a mechano-chemically treated indium−gallium−zinc oxide (IGZO) absorption layer is reported. Through this novel and facile mechano-chemical treatment, mechanical removal of the cellophane adhesive tape induces reactive radicals and organic compounds on the sputtered IGZO film surface. Surface modification, following the mechano-chemical treatment, caused porous sites in the solution-processed IGZO film, which can give rise to a homojunction-porous IGZO (HPI) layer and generate sub-gap states from oxygen-related defects. These intentionally generated sub-gap states played a key role in photoelectron generation under illumination with relatively long-wavelength visible light despite the wide band gap of IGZO (>3.0 eV). Compared with conventional IGZO phototransistors, our HPI phototransistor displayed outstanding optoelectronic characteristics and sensitivity; we measured a threshold voltage (V_{th}) shift from 3.64 to −6.27 V and an on/off current ratio shift from 4.21×10^{10} to 4.92×10^{2} under illumination with a 532 nm green light of 10 mW/mm^2 intensity and calculated a photosensitivity of 1.16×10^{8}. The remarkable optoelectronic characteristics and high optical transparency suggest optical sensor applications.

KEYWORDS: *phototransistors, oxide thin-film transistors, indium gallium zinc oxide, mechano-chemical treatment, sub-gap states*

Downloaded via YONSEI UNIV on November 26, 2021 at 05:31:09 (UTC).
See https://pubs.acs.org/sharingguidelines for options on how to legitimately share published articles.

1. INTRODUCTION

Optical sensors are analytical devices used to measure a physical quantity of light by converting light rays into an electronic signal. Depending on the type of the sensor, various methods are used to translate the signal into a form that is readable by an integrated measuring device, such as photovoltaic and photoconductive devices, photodiodes, and phototransistors. Potential applications include the full range of analytical tasks, from mobile devices that can control screen brightness to vehicles, cameras, and medical devices.[1−4]

Nowadays, the constant growth of interest in the field of optical sensors has been observed in almost every commercial application. Conventional hydrogenated amorphous silicon (a-Si:H) thin-film phototransistors can serve as detecting elements in contact image sensors and as optical feedback elements in diverse types of displays.[5] Meanwhile, more challenging types of sensors have also been recently reported. For example, several graphene-based nanomaterials and organic heterostructured materials have been developed, and their electronic performance and photodetection potential have been unveiled in many research studies.[6,7] As a natural consequence, these advances in interdisciplinary research studies and industrial approaches have practically improved the optical characteristics of various types of photonic devices comparable to those of conventional Si-based photosensors.[8,9]

Among these various sensing materials, metal-oxide semiconductors are considered to be the most appropriate materials

Received: May 15, 2021
Accepted: July 15, 2021
Published: July 23, 2021

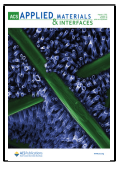

© 2021 American Chemical Society

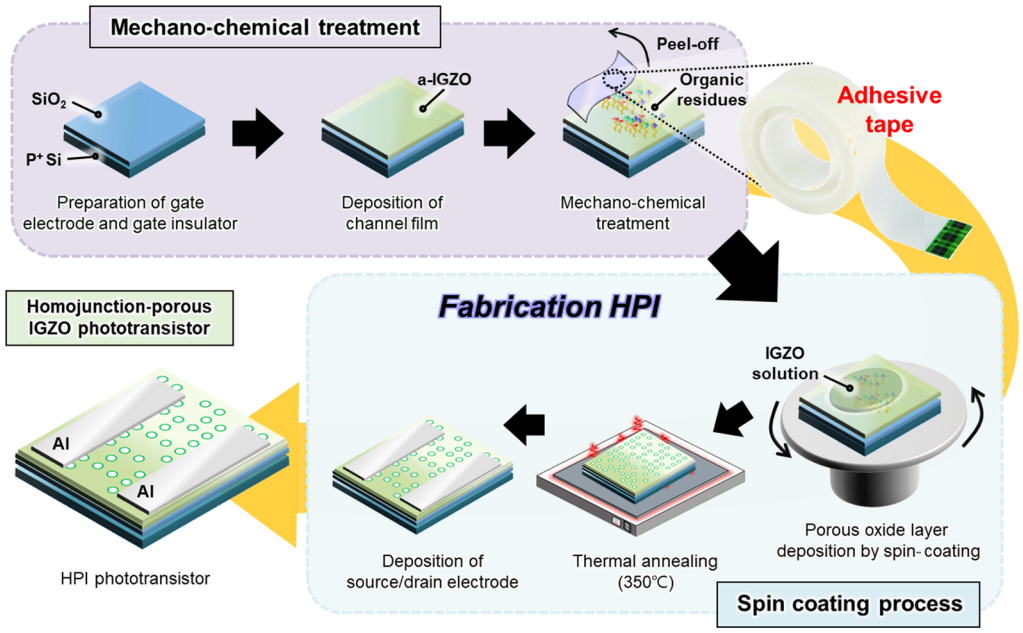

Figure 1. Schematic diagram of the fabrication process of homojunction-porous IGZO (HPI)-based phototransistor.

for photodetectors because of their wide range of electronic and optical properties, for example, high-field-effect mobility, low off-state current, optical transparency, and processing versatility.[10,11] In particular, metal-oxide thin-film transistors (TFTs) are particularly promising candidates because their fabrication process is easily compatible with the existing TFT technology in the display industry.[12]

However, the wide band gap over 3.0 eV of the metal-oxide channel layer restricts its possible absorption range to a thickness of less than ~420 nm, which corresponds to the wavelengths of ultraviolet and blue light. Although a few excited electrons are generated in the oxygen-related sub-gap states in metal-oxide films, their density does not provide sufficient sensitivity.

In this respect, several studies have broadened the light absorption range of metal-oxide-based phototransistors over the years. Most approaches have adopted heterogeneous metal-oxide structures containing additional light-absorbing layers, such as nanostructures or two-dimensional materials.[13,14] However, using these narrow band gap materials causes concomitant limitations of large-area deposition and also additional fabrication cost. To overcome these limitations, many studies have proposed indium−gallium−zinc oxide (IGZO) phototransistors with various light absorption layers for the detection of long wavelengths of visible light.[15−17]

Herein, we describe a novel homojunction-porous IGZO (HPI) phototransistor; the sub-gap states of the back channel of these phototransistors were modulated via a mechano-chemical treatment for broad-light absorption.[18] Through this technique, we demonstrated various merits of the HPI phototransistor including low production costs, good reproducibility, and broad adaptability, accelerating the realization of a photosensing system that can be adopted in the existing applications to enhance its sensitivity and stability.[19]

2. EXPERIMENTAL SECTION

2.1. Preparation of the IGZO Solution. For the solution-processed oxide thin-film-based light absorption layer, synthesis of the 0.3 M solution should be undertaken first. Indium nitrate hydrate [$In(NO_3)_3{\cdot}xH_2O$], zinc nitrate hexahydrate [$Zn(NO_3)_2{\cdot}6H_2O$], and gallium nitrate hydrate [$Ga(NO_3)_3{\cdot}xH_2O$] were chosen as precursors to prepare the IGZO solution. The precursors were dissolved in a solvent, 2-methoxy ethanol (2ME), and then nitric acid was added in a dropwise manner to control the acidity of the solution and synthesize a homogeneous solution. The mixture was stirred for 4 h at 35 °C and aged for another 24 h at room temperature to obtain the IGZO solution at a In/Ga/Zn molar ratio of 5:1:2.

2.2. Fabrication of IGZO Phototransistors. The phototransistors described in this paper had a bottom-gate, top-contact TFT structure with the HPI (Figure 1). First, a heavily p-type-doped Si wafer, on which a 1200 Å thick SiO_2 layer had been thermally grown, was used as the device substrate. The IGZO channel was deposited with a shadow mask onto a sputtering target of In_2O_3−Ga_2O_3−ZnO at a 1:1:1 molar ratio, via radiofrequency magnetron sputtering at 150 W and 5.0×10^{-3} Torr for 5 min at room temperature. The deposited IGZO film was then mechano-chemically treated by placing the adhesive side of the cellophane tape on it for 1 s and then peeling off the tape, which left organic residues on the surface.

Then, the synthesized IGZO solution was spin-coated onto the surface at 3000 rpm for 30 s, and the assembly was then pre-annealed at 100 °C for 10 min and finally post-annealed at 350 °C for 1 h to obtain the HPI film. Source and drain electrodes having a length of 150 μm and a width of 1000 μm were deposited by Al thermal evaporation to complete the HPI phototransistor.

For comparison, two types of IGZO thin films, a sputtered IGZO film (single IGZO) and a multilayer of sputtered IGZO and solution-processed IGZO (sputtered and solution-processed IGZO, SSI), were prepared and examined. Besides, phototransistors with these IGZO thin films were fabricated using exactly the same fabrication process mentioned earlier except for the channel layer.

2.3. Characterization of Phototransistors. For surface analysis of the HPI, the morphologies were scanned via atomic force microscopy (AFM) (model NX-10; Park Systems). Images of the HPI were taken by a field-emission scanning electron microscope (model JSM-7001F; JEOL). The chemical properties of the HPI were analyzed by X-ray photoelectron spectroscopy (XPS) (model K-Alpha; Thermo Fisher Scientific) and Fourier transform infrared (FT-IR) spectroscopy (model Vertex 70, Bruker). The work function and electronic band structures with sub-gap states were calculated using ultraviolet−visible (UV−vis) spectroscopy (Lambda 750; ULVAC PHI) and UV photoelectron spectroscopy (UPS) (model AXIS

https://doi.org/10.1021/acsami.1c09012
ACS Appl. Mater. Interfaces 2021, 13, 35981−35989

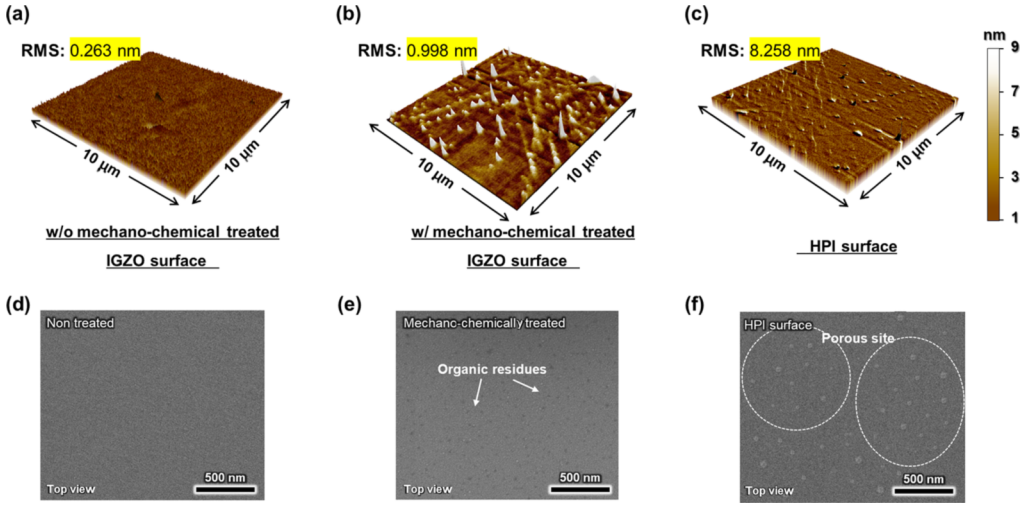

Figure 2. AFM images of the IGZO surface (a) without and (b) with mechano-chemical treatment, and (c) the HPI surface. SEM images of the IGZO surface (d) without and (e) with mechano-chemical treatment and (f) the HPI surface.

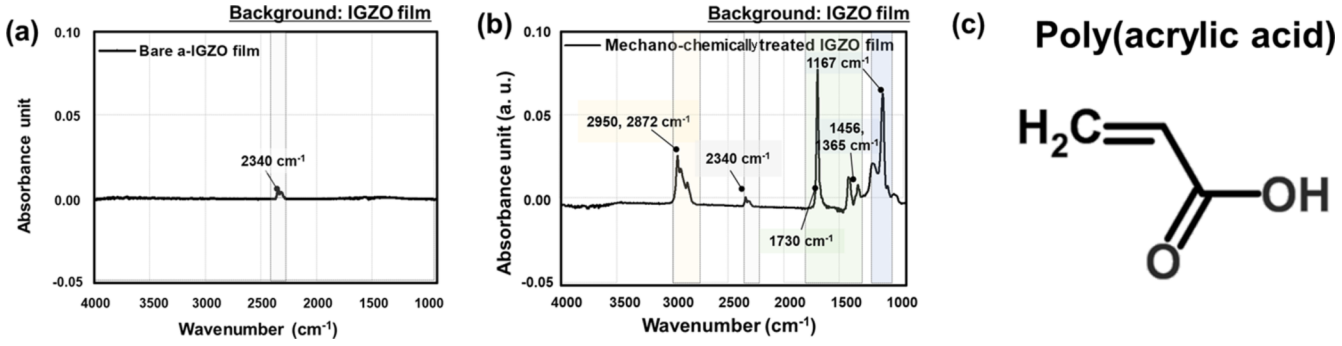

Figure 3. FT-IR spectra of the IGZO thin film (a) before and (b) after mechano-chemical treatment. (c) Schematic illustration of polyacrylate on an adhesive tape.

Supra; Kratos), respectively. The optoelectronic characteristics of IGZO phototransistors were measured using a semiconductor parameter analyzer (model HP 4156C; Agilent Technologies). The transfer curve was performed at a fixed drain voltage (V_{DS}) of 10.1 V and a gate voltage (V_{GS}) swept from −30 to +30 V. First, the initial states were measured out in a dark box under ambient conditions and then compared with the measurements under light exposure. The sources of light illumination used in this report were monochromic lasers of red (635 nm), green (532 nm), and blue (405 nm).

3. RESULTS AND DISCUSSION

For analysis of surface morphology, Figure 2a−c shows three-dimensional AFM images of the 10 × 10 μm^2 area of IGZO thin films before and after mechano-chemical treatment and of the HPI thin film. As a result, we completely verified that some dots were observed on the surface of the IGZO thin film after the mechano-chemical treatment and calculated the root-mean-square (rms) roughness values to be 0.263 and 0.998 in the images shown in Figure 2a,b, respectively. We attributed these sharp peaks to the organic residue from the adhesive tape. Interestingly, as shown in Figure 2c, the surface of the IGZO thin film was completely changed to show a morphology that appears to be perforated in many places (i.e., rms roughness is 8.258 nm). Similarly, the SEM images shown in Figure 2d−f confirm that surface modification occurred during the HPI fabrication process. We believe that these dots (i.e., traces of organic residue) inhibited the uniform deposition of the solution during the spin-coating process, which led to voids in the coating. Accordingly, morphology modification due to mechano-chemical treatment resulted in a rougher surface and porous sites after the formation of the HPI layer. Furthermore, the organic residues were not observed after thermal annealing at 350 °C, which indicated that the HPI process caused the residues to disappear (Figures S1−S3, Supporting Information).

To verify the precise composition of the surface residues left by the mechano-chemical treatment, FT-IR spectroscopy was carried out with the IGZO thin film before and after the treatment, as depicted in Figure 3a,b. The spectrum of the as-deposited IGZO thin film showed only a minor peak at 2340 cm^{-1}, corresponding to CO_2; this peak commonly appears whenever FT-IR analysis is performed in an air atmosphere. However, the spectrum of the mechano-chemically treated IGZO thin film displayed broad peaks at 2950 and 2872 cm^{-1}, corresponding to C−H stretching vibrations. The peak at 1730 cm^{-1} was assigned to the C═O stretching vibration and those at 1456, 1365 cm^{-1} (C═O), and 1167 cm^{-1} (C−O) to the COO moiety. Together, these peaks confirmed the transfer of organic residue from the adhesive tape during the mechano-chemical treatment. The FT-IR signals were consistent with the polyacrylate group (Figure 3c).[20,21]

To evaluate the sensitivity of the HPI phototransistors, we measured the transfer characteristics of phototransistors upon light exposure at a V_{DS} of 10.1 V with varying light intensities of 1, 5, and 10 mW/mm^2, as represented in Figure 4. In the

https://doi.org/10.1021/acsami.1c09012
ACS Appl. Mater. Interfaces 2021, 13, 35981−35989

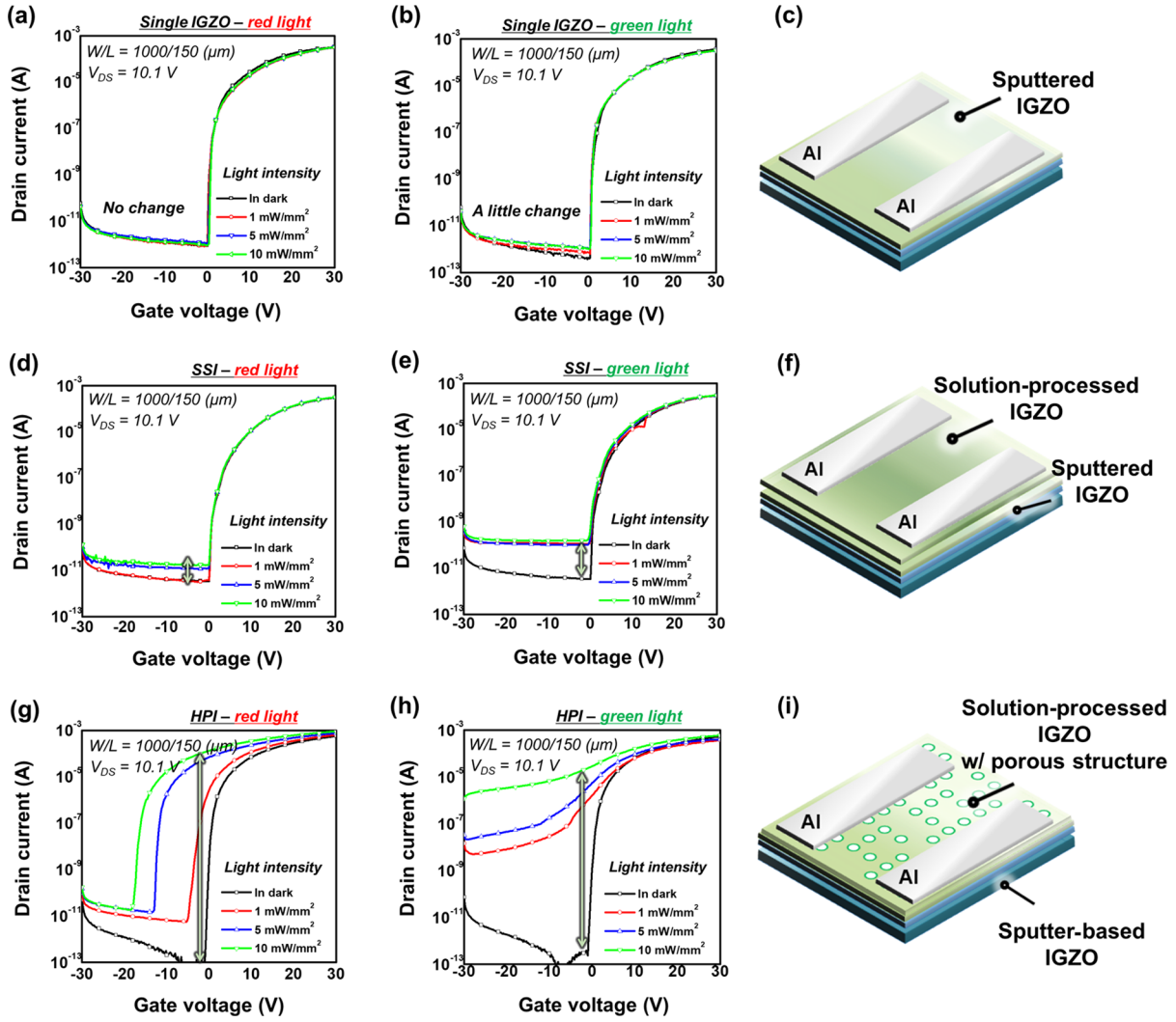

Figure 4. Transfer characteristics of phototransistors fabricated using (a) single IGZO, (d) SSI, and (g) HPI thin films under exposure to red light and (b) single IGZO, (e) SSI, and (h) HPI under exposure to green light. Schematic illustration of the structure of devices fabricated from (c) single IGZO, (f) SSI, and (i) HPI thin films.

Table 1. Optoelectronic Parameters of Oxide Phototransistors Fabricated Using Single IGZO, SSI, and HPI Thin Films in the Dark and upon Exposure to Green Light

	in the dark				in green light (10 mW/mm^2)				
sample	μ_{FE} (cm^2 V^{-1} s^{-1})	V_{th} (V)	S.S. (V dec^{-1})	on/off current ratio	μ_{FE} (cm^2 V^{-1} s^{-1})	V_{th} (V)	S.S. (V dec^{-1})	on/off current ratio	photosensitivity
single IGZO phototransistor	10.88	4.71	0.35	1.01×10^9	9.53	3.99	0.36	3.23×10^8	no change
SSI phototransistor	11.34	5.68	0.43	9.16×10^8	9.79	2.87	0.28	2.00×10^6	1.74×10^2
HPI phototransistor	12.64	3.64	0.40	4.21×10^{10}	11.98	−6.27	8.69	4.92×10^2	1.63×10^{10}

Supporting Information (Figure S5), there are results of blue light conditions from several single IGZO, SSI, and HPI phototransistors. Despite the wide band gap above 3.0 eV of IGZO, our phototransistor clearly absorbed certain regions of the light illumination spectrum. In general, phototransistors tend to be more conductive concomitant to a negative shift of the threshold voltage (V_{th}) and an increase of the off state current under light. These characteristics become more marked with increasing light intensity.[22] Specifically, in the case of the IGZO TFT with HPI, the V_{th} and the on/off current ratio shifted from 3.64 to −6.27 V and from 4.21×10^{10} to 4.92×10^2, respectively, under a green light of 10 mW/mm^2, ensuring a reasonable photosensitivity of 1.63×10^{10}. There are some comparisons of photosensing characteristics in the Supporting Information (Table S1).

On the other hand, TFTs containing single IGZO and SSI films with wide band gaps displayed no change, or only a slight increase in the off current. The photosensitivity with respect to sweeping V_{GS} and fixed V_{DS} was calculated using the following equation:

$$R = \frac{J_{photo}}{P_{light}} = \frac{(I_{light} - I_{dark})/A_{photo}}{P_{light}/A_{laser}}$$

https://doi.org/10.1021/acsami.1c09012
ACS Appl. Mater. Interfaces 2021, 13, 35981−35989

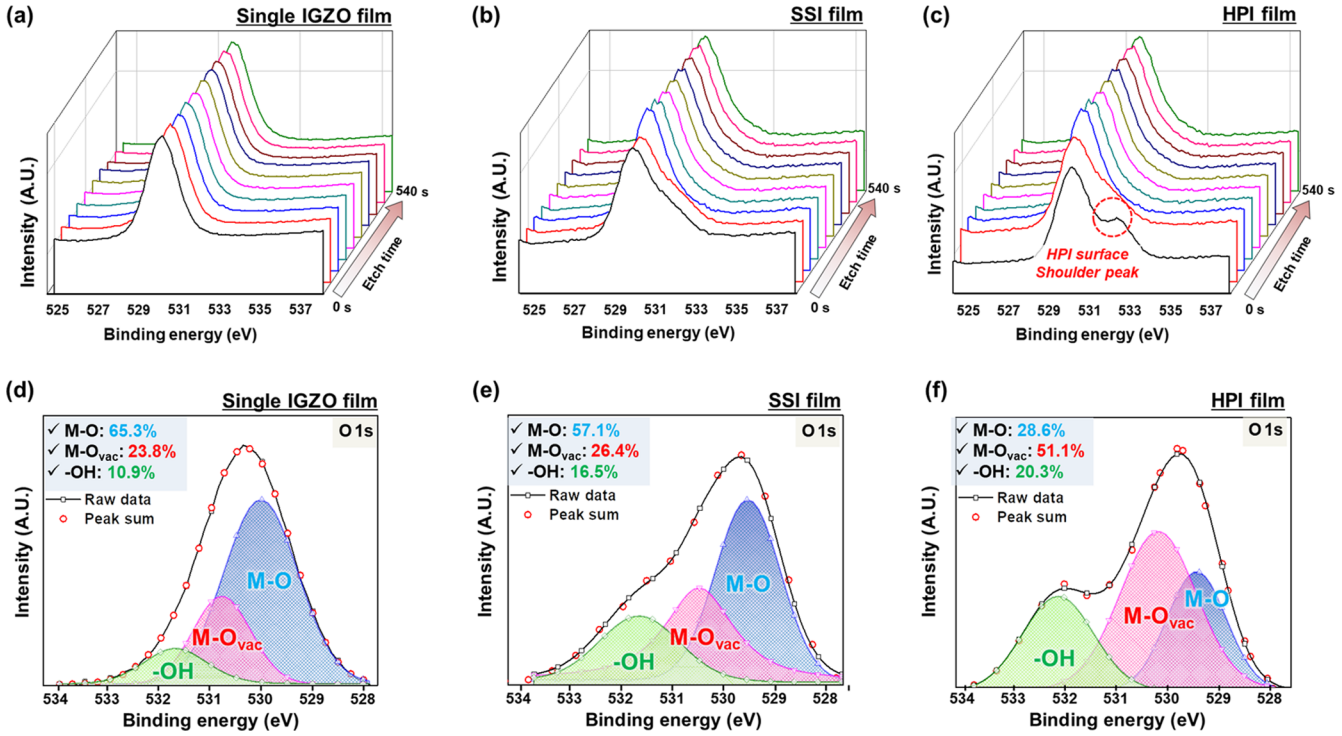

Figure 5. XPS results of (a) single IGZO, (b) SSI, and (c) HPI as a function of the etch time; deconvoluted O 1s spectra of (d) single IGZO, (e) SSI, and (f) HPI films.

where J_{photo} is the photocurrent density, P_{light} is the incident light power density, I_{light} is the drain current under light illumination, I_{dark} is the current under dark conditions, A_{photo} is the product of the channel width and thickness, and A_{laser} (i.e., 0.15 mm^2, channel width × length) is the diameter of the laser source.[23−25] Table 1 summarizes all the detailed variations of characteristics suggesting the superior photosensitivity of HPI phototransistors. In the Supporting Information (Figures S4 and S12), there are more detailed statistical data of field-effect mobility, on/off current ratio, and photosensitivity of several single IGZO, SSI, and HPI phototransistors.

Among the IGZO-based phototransistors, the HPI-based one was notably high-performing. XPS was used to substantiate the enhanced optoelectronic characteristics, in terms of chemical and structural compositions, of the HPI. Figure 5 depicts the variations of O 1s peaks of three types of thin films, single IGZO, SSI, and HPI under the etching process. Note that the disappearance of a shoulder peak at a depth of about 20 nm was clearly observed in the case of HPI (more details of the thickness profile is provided in the Supporting Information, Figure S8). The O 1s peaks were deconvoluted into three peaks at 530.3 ± 0.2, 531.2 ± 0.2, and 532.1 ± 0.2 eV, related to metal−oxygen bonding (M−O), oxygen vacancy (M−O_{vac}), and hydroxide species (−OH), respectively, by Gaussian distributions.[26,27] Specifically, the M−O peak represents conducting pathways for electrons in IGZO. Meanwhile, M−O_{vac} is known to be associated with the oxygen vacancies, and the −OH peak is attributed to the metal hydroxide or metal oxide−carbon (M−OC) groups containing organic residues. In this regard, significant increases of the M−O_{vac} peak and the −OH peak of HPI (M−O: 28.6%, M−O_{vac}: 51.1%, −OH: 20.3%) determine the overall increase of impurities, which generate trap sites compared with the single IGZO or SSI film.[28] For more detailed peak analysis, we interpreted the photosensitivity of HPI as a result of the alteration of the chemical composition associated with the remaining polyacrylate groups on the IGZO surface after the mechano-chemical treatment that supplied additional states in the band gap.[29,30] Note that the change in the chemical composition seems to occur from the surface to a depth of about 20 nm of the HPI layer. This region plays a key role in photocurrent in which most trap-assisted excitons generated act as a light absorption layer. We interpret this phenomenon as a result of the mechano-chemical treatment associated with the organic residues of the HPI layer, which generate sub-gap states in the porous layer for visible light absorption and electron−hole pair generation. Besides, no chemical composition was observed underneath 20 nm of the light absorption layer, and we conjectured that this channel layer secures a reasonable carrier diffusion length.

Through these results, two possible roles of holes in the porous layer could be explained as follows: (1) generation of photocurrent and (2) enhancement of the absorption efficiency. In the generation of photocurrent, physical defects, such as micro-/nanosized holes or cracks in the film, can impact the photocatalytic activity and electron transport.[31,32] Moreover, various research studies showing that the pore sites in the thin film act as defect sites, generating unstable bonds, have been reported.[33,34] Therefore, we assumed that the physical defect (e.g., hole) in the porous film can generate weak metal−oxygen binding and also create oxygen-related defects (i.e., oxygen vacancy) due to the stabilized state. As shown in XPS depth analysis, we can conclude that the holes in the porous layer can give rise to an increase in the oxygen vacancy (Figure S6, Supporting Information). Next, we explain the role of oxygen vacancies in oxide phototransistors. It is widely known that as oxygen vacancies are formed within the layer of the oxide phototransistors, more sub-gap states are

https://doi.org/10.1021/acsami.1c09012
ACS Appl. Mater. Interfaces 2021, 13, 35981−35989

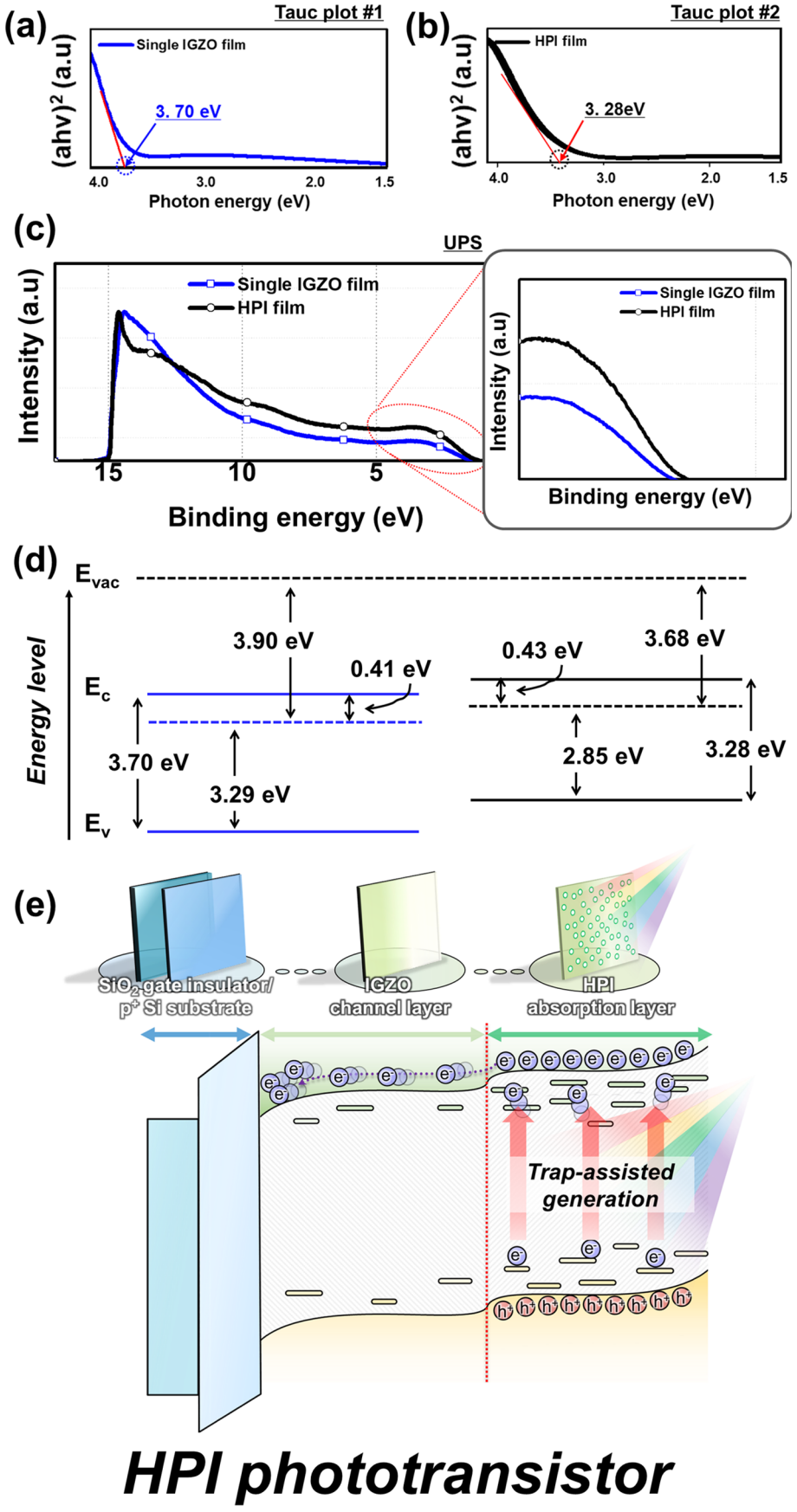

Figure 6. Tauc plot results: (a) single IGZO film and (b) HPI film. (c) UPS results of single IGZO and HPI films. (d) Schematic diagram of the band structure before junction. (e) Illustration of trap-assisted generation and electron transport of the IGZO phototransistor with the HPI absorption layer.

https://doi.org/10.1021/acsami.1c09012
ACS Appl. Mater. Interfaces 2021, 13, 35981−35989

created within the band gap of the phototransistors.[15] Owing to these properties, our phototransistors could absorb the light through the abundant number of sub-gap states, which repeatedly trap and excite electrons and contribute them to the photocurrent. In addition, in the field of photo-electrochemical (PEC) research, various studies have been conducted in which such physical defects increase the surface area that enables responding to external factors (light, gas, and biomarker etc.).[35−37] Moreover, to improve the absorption efficiency, some researchers have introduced scattering layers using a porous layer.[38] Therefore, it can be considered that these holes in the porous layer played a role not only in response to light but also in enhancing the absorption efficiency.

This hypothesis of induced sub-gap states was supported by converging pieces of evidence, such as the results of the UV−vis absorption and UPS results. We compared the light absorption characteristics of two types of IGZO thin films; single IGZO and HPI films, in terms of energy band structures and sub-gap states. Tauc plots and band gaps were calculated from UV−vis absorption data as represented in Figure 6a,b, which showed band gaps of single IGZO and HPI of 3.70 and 3.53 eV, respectively. This difference of 0.17 eV in the band gap guarantees the aforesaid chemical composition variation caused by the mechano-chemical treatment. A slightly narrow but still wide band gap of the HPI improved the absorption of visible light of long wavelengths compared with single IGZO, retaining its transparent characteristics.[39,40] Additionally, the comparison of the Tauc plot (i.e., UV−visible) results is included in the Supporting Information (Figure S7).

The UPS results of Figure 6c indicate the cutoff energies of 17.02 and 18.24 eV and valence band maximum (VBM) energy levels of 3.29 and 2.85 eV, for single IGZO and HPI films, respectively. The relatively higher intensity of the HPI case compared with the single IGZO film near the VBM level represents clear evidence of the presence of sub-gap states deliberately generated during the mechano-chemical treatment.[41,42] The energy band structure was calculated based on these data using the following equation[43]:

$$\Phi = h\nu - |E_{cutoff} - E_F|$$

where Φ is the work function, $h\nu$ is the incident light energy, E_{cutoff} is the cutoff energy, and E_F is the Fermi level. In detail, a single IGZO film had a work function of 3.90 eV and a conduction band minimum (CBM) energy level of 3.29 eV. On the other hand, HPI showed a work function of 3.68 eV and a CBM energy level of 3.28 eV, as described in Figure 6d.

Herein, we demonstrated that the energy-band alignment of the HPI phototransistor correspond to the aforementioned UPS results that showed that HPI was composed of two types of sub-layers, an upper part of the chemically modified region and a lower part of the single IGZO region. In the UPS analysis, these spectra were obtained using He irradiation with $h\nu$ = 21.21 eV produced by a UV source and a voltage bias with −5.0 eV. Figure 6e shows the band structure analysis of the HPI phototransistor operating under visible light illumination. The band offset between the CBM energy level of the sub-layers was 0.10 eV, and this minimal difference improved the electron transport in HPI.

In summary, electrons in the valence band were excited and trapped in the sub-gap states and readily excited in the light absorption layer of the conduction band with relatively low photon energy. The traps assisted in the production of photocurrent by acting as electron−hole pair generation centres, and the photoelectrons were then easily transported through the channel layer. A detailed description of the UPS results is provided in the Supporting Information (Figure S9).

Finally, as shown in Figure S10 (Supporting Information), we conducted the measurements at V_G = −1.0 V and V_D = 10.1 V for 3600 s (switching the same green laser illumination conditions at 0.02 Hz). As a result, the device exhibited moderate, durable, and clearly switching characteristics between the on and off states.

4. CONCLUSIONS

In summary, we have demonstrated a new concept of the HPI phototransistor based on the mechano-chemical treatment. The HPI was composed of an upper part, 20 nm thickness of the light absorption region, and a lower part, 40 nm thickness of the IGZO channel region. Specifically, the light absorption layer was mechano-chemically modified with artificially generated oxygen-related subgap states, which play an important role in the trap-assisted generation of excited electrons. This guarantees the broad absorption range including from UV and visible light regions. In addition, under IGZO, the channel region provided a reasonable carrier diffusion length. Compared with conventional IGZO-based phototransistors, the HPI phototransistor exhibited superior optoelectronic characteristics and photosensitivity with a shift of V_{th} and on/off current ratio from 3.64 to −6.27 V and from 4.21 × x10^{10} to 4.92 × x10^{2}, respectively, and a calculated photosensitivity of 1.63 × 10^{10}, under a green light of 10 mW/mm^2. As a result, we suggest that highly transparent visible-light photosensors can be applicable to the conventional optical sensor design.

■ ASSOCIATED CONTENT

Supporting Information

The Supporting Information is available free of charge at https://pubs.acs.org/doi/10.1021/acsami.1c09012.

SEM, FT-IR, and AFM images of IGZO and treated IGZO films; statistical data of the IGZO, SSI, and HPI phototransistors; XPS depth profile; comparison of UV−visible results according to the device structure; depth profile according to the concentration of IGZO solution confirmed by ellipsometry analysis; raw data of UPS analysis; long-term endurance test for stability; schematic diagram of treatment equipment for uniformity; and photoresponsivity according to the gate voltage and light intensity (PDF)

■ AUTHOR INFORMATION

Corresponding Author

Hyun Jae Kim − *School of Electrical and Electronic Engineering, Yonsei University, Seoul 03722, Republic of Korea;* orcid.org/0000-0002-6879-9256; Email: hjk3@yonsei.ac.kr

Authors

I. Sak Lee − *School of Electrical and Electronic Engineering, Yonsei University, Seoul 03722, Republic of Korea;* orcid.org/0000-0002-6616-189X

Joohye Jung − *School of Electrical and Electronic Engineering, Yonsei University, Seoul 03722, Republic of Korea; Display*

R&D Center, Samsung Display Co., Ltd., Asan-Si 31454, Republic of Korea

Dong Hyun Choi − *School of Electrical and Electronic Engineering, Yonsei University, Seoul 03722, Republic of Korea*

Sujin Jung − *School of Electrical and Electronic Engineering, Yonsei University, Seoul 03722, Republic of Korea*

Kyungmoon Kwak − *School of Electrical and Electronic Engineering, Yonsei University, Seoul 03722, Republic of Korea*

Complete contact information is available at: https://pubs.acs.org/10.1021/acsami.1c09012

Author Contributions

§I.S.L. and J.J. contributed equally.

Notes

The authors declare no competing financial interest.

■ ACKNOWLEDGMENTS

This work was supported by the Technology Innovation Program (20010371, Development of 4K level flexible display device and panel technology by the inkjet pixel printing method) funded by the Ministry of Trade, Industry & Energy (MOTIE, Korea).

■ REFERENCES

(1) Xie, C.; Liu, C. K.; Loi, H. L.; Yan, F. Perovskite-Based Phototransistors and Hybrid Photodetectors. *Adv. Funct. Mater.* **2020**, *30*, 1903907.

(2) Bethke, K.; Palantöken, S.; Andrei, V.; Roß, M.; Raghuwanshi, V. S.; Kettemann, F.; Greis, K.; Ingber, T. T. K.; Stückrath, J. B.; Valiyaveettil, S.; Rademann, K. Functionalized Cellulose for Water Purification, Antimicrobial Applications, and Sensors. *Adv. Funct. Mater.* **2018**, *28*, 1800409.

(3) Rim, Y. S. Review of Metal Oxide Semiconductors-Based Thin-Film Transistors for Point-of-Care Sensor Applications. *J. Inf. Disp.* **2020**, *21*, 203−210.

(4) Damulira, E.; Yusoff, M. N. S.; Omar, A. F.; Mohd Taib, N. H. A Review: Photonic Devices Used for Dosimetry in Medical Radiation. *Sensors* **2019**, *19*, 2226.

(5) Nascetti, A.; Caputo, D. Amorphous Silicon Phototransistor as Nonlinear Optical Device for High Dynamic Range Imagers. *IEEE Electron Device Lett.* **2002**, *49*, 395−399.

(6) Kang, B. H.; Jung, S. J.; Hong, S.; Lee, I. S.; Hong, S.; Kim, S.; Kim, H. J. Improvement of the Stability and Optoelectronic Characteristics of Molybdenum Disulfide Thin-Film Transistors by Applying a Nitrocellulose Passivation Layer. *J. Inf. Disp.* **2020**, *21*, 123−130.

(7) Tian, W.; Zhou, H.; Li, L. Hybrid Organic-Inorganic Perovskite Photodetectors. *Small* **2017**, *13*, 1702107.

(8) Yu, Y.; Zhang, Y.; Zhang, Z.; Zhang, H.; Song, X.; Cao, M.; Che, Y.; Dai, H.; Yang, J.; Wang, J.; Zhang, H.; Yao, J. Broadband Phototransistor Based on $CH_3NH_3PbI_3$ Perovskite and PbSe Quantum Dot Heterojunction. *J. Phys. Chem. Lett.* **2017**, *8*, 445−451.

(9) Zhang, Y.; Qian, L.-X.; Wu, Z.; Liu, X. Amorphous InGaMgO ultraviolet Photo-TFT with Ultrahigh Photosensitivity and Extremely Large Responsivity. *Materials* **2017**, *10*, 168.

(10) Knobelspies, S.; Daus, A.; Cantarella, G.; Petti, L.; Münzenrieder, N.; Tröster, G.; Salvatore, G. A. Flexible a-IGZO Phototransistor for Instantaneous and Cumulative UV-Exposure Monitoring for Skin Health. *Adv. Electron. Mater.* **2016**, *2*, 1600273.

(11) Chang, S.-P.; Hua, W.-C.; Li, J.-Y. High Responsivity Indium-Zinc-Oxide Ultraviolet Thin-Film Phototransistor. *J. Nanosci. Nanotechnol.* **2017**, *17*, 4864−4866.

(12) Chang, T. H.; Chiu, C. J.; Weng, W. Y.; Chang, S. J.; Tsai, T. Y.; Huang, Z. D. High Responsivity of Amorphous Indium Gallium Zinc Oxide Phototransistor with Ta_2O_5 Gate Dielectric. *Appl. Phys. Lett.* **2012**, *101*, 261112.

(13) Ahn, C. H.; Kim, Y. K.; Kang, W. J.; Kim, K. S.; Cho, H. K. High Photosensitivity and Wide Operation Voltage in Two-dimensional CdS Nano-crystal Layer Embedded a-InGaZnO Hybrid Phototransistors. *J. Alloys Compd.* **2017**, *725*, 891−898.

(14) Yu, J.; Kim, B. J.; Park, S.; Han, I. K.; Kang, S. J. Red/green/blue Selective Phototransistors with a Hybrid Structure of Quantum-dots and an Oxide Semiconductor. *Jpn. J. Appl. Phys.* **2018**, *57*, 044001.

(15) Chung, J.; Tak, Y. J.; Kim, W.-G.; Kang, B. H.; Kim, H. J. Artificially Fabricated Subgap States for Visible-Light Absorption in Indium-Gallium-Zinc Oxide Phototransistor with Solution-Processed Oxide Absorption Layer. *ACS Appl. Mater. Interfaces* **2019**, *11*, 38964−38972.

(16) Hsiao, Y.-H.; Leung, T.-P.; Li, J.-T.; Shih, L.-C.; Chen, J.-S. Charge Trapping Augmented Switchable Sub-band-gap Photo response of Zinc−Tin Oxide Thin-Film Transistor. *ACS Appl. Electron. Mater.* **2020**, *2*, 2078−2083.

(17) Kang, B. H.; Kim, W.-G.; Chung, J.; Lee, J. H.; Kim, H. J. Simple Hydrogen Plasma Doping Process of Amorphous Indium Gallium Zinc Oxide-Based Phototransistors for Visible Light Detection. *ACS Appl. Mater. Interfaces* **2018**, *10*, 7223−7230.

(18) Lee, I. S.; Tak, Y. J.; Kang, B. H.; Yoo, H.; Jung, S.; Kim, H. J. Mechanochemical and Thermal Treatment for Surface Functionalization to Reduce the Activation Temperature of In-Ga-Zn-O Thin-film Transistors. *ACS Appl. Mater. Interfaces* **2020**, *12*, 19123.

(19) Kowalewska, A.; Nowacka, M.; Tracz, A.; Makowski, T. Supramolecular Self-Assembly of Linear Oligosilsesquioxanes on Mica-AFM Surface Imaging and Hydrophilicity Studies. *Soft Matter* **2015**, *11*, 4818.

(20) Jiao, G.; Yu, G.; Wang, W.; Zhao, X.; Zhang, J.; Ewart, S. H. Properties of Polysaccharides in Several Seaweeds from Atlantic Canada and Their Potential Anti-Influenza Viral Activities. *J. Ocean Univ. China* **2012**, *11*, 205.

(21) Sabri, M. M.; Jung, J.; Yoon, D. H.; Yoon, S.; Tak, Y. J.; Kim, H. J. Hydroxyl Radical-assisted Decomposition and Oxidation in Solution-processed Indium Oxide Thin-Film Transistors. *J. Mater. Chem. C* **2015**, *3*, 7499.

(22) Abe, K.; Nomura, K.; Kamiya, T.; Hosono, H. Optical Evidence for Quantization in Transparent Amorphous Oxide Semiconductor Superlattice. *Phys. Rev. B* **2012**, *86*, 081202.

(23) Qian, G.; Qi, J.; Davey, J. A.; Wright, J. S.; Wang, Z. Y. Family of Diazapentalene Chromophores and Narrow Band Gap Polymers: Synthesis, Halochromism, Halofluorism, and Visible Near Infrared Photodetectivity. *Chem. Mater.* **2012**, *24*, 2364.

(24) Gong, X.; Tong, M.; Xia, Y.; Cai, W.; Moon, J. S.; Cao, Y.; Yu, G.; Shieh, C.-L.; Nilsson, B.; Heeger, A. J. High Detectivity Polymer Photodetectors with Spectral Response from 300 nm to 1450 nm. *Science* **2009**, *325*, 1665.

(25) Mottram, A. D.; Lin, Y.-H.; Pattanasattayavong, P.; Zhao, K.; Amassian, A.; Anthopoulos, T. D. Quasi Two-Dimensional Dye-Sensitized In_2O_3 Phototransistors for Ultrahigh Responsivity and Photosensitivity Photodetector Applications. *ACS Appl. Mater. Interfaces* **2016**, *8*, 4894.

(26) Jang, J.; Kang, Y.; Cha, D.; Bae, J.; Lee, S. Thin-Film Optical Devices Based on Transparent Conducting Oxides: Physical Mechanisms and Applications. *Crystals* **2019**, *9*, 192.

(27) Chung, J.; Tak, Y. J.; Kim, W.-G.; Park, J. W.; Kim, T. S.; Lim, J. H.; Kim, H. J. Low-temperature Fabrication of Solution-processed Hafnium Oxide Gate Insulator Films using a Thermally Purified Solution Process. *J. Mater. Chem. C* **2018**, *6*, 4928.

(28) Ahn, S.-E.; Song, I.; Jeon, S.; Jeon, Y. W.; Kim, Y.; Kim, C.; Ryu, B.; Lee, J.-H.; Nathan, A.; Lee, S.; Kim, G. T.; Chung, U.-I. Metal Oxide Thin Film Phototransistor for Remote Touch Interactive Displays. *Adv. Mater.* **2012**, *24*, 2631.

(29) Denny, Y. R.; Shin, H. C.; Seo, S.; Oh, S. K.; Kang, H. J.; Tahir, D.; Heo, S.; Chung, J. G.; Lee, J. C.; Tougaard, S. Electronic and

Optical Properties of Hafnium Indium Zinc Oxide Thin Film by XPS and REELS. *J. Electron Spectrosc. Relat. Phenom.* **2012**, *185*, 18.
(30) Flynn, B. T.; Oleksak, R. P.; Thevuthasan, S.; Herman, G. S. Interfacial Chemistry-induced Modulation of Schottky Barrier Heights: In Situ Measurements of the Pt-Amorphous Indium Gallium Zinc Oxide Interface using X-ray Photoelectron Spectroscopy. *ACS Appl. Mater. Interfaces* **2018**, *10*, 4333.
(31) Liu, R.; Lin, Y.; Chou, L.-Y.; Sheehan, S. W.; He, W.; Zhang, F.; Hou, H. J. M.; Wang, D. Water Splitting by Tungsten Oxide Prepared by Atomic Layer Deposition and Decorated with an Oxygen-Evolving Catalyst. *Angew. Chem., Int. Ed.* **2011**, *50*, 499.
(32) Zhu, T.; Chong, M. N.; Chan, E. S. Nanostructured Tungsten Trioxide Thin Films Synthesized for Photo Electrocatalytic Water Oxidation: A Review. *ChemSusChem* **2014**, *7*, 2974.
(33) Jeong, D.-W.; Kim, K. H.; Kim, B. S.; Byun, Y. T. Characteristics of Highly Sensitive and Selective Nitric Oxide Gas Sensors Using Defect-Functionalized Single-Walled Carbon Nanotubes at Room Temperature. *Appl. Surf. Sci.* **2021**, *550*, 149250.
(34) Zhang, Z.; Lu, L.; Lv, Z.; Chen, Y.; Jin, H.; Hou, S.; Qiu, L.; Duan, L.; Liu, J.; Dai, K. Porous Carbon Nitride with Defect Mediated Interfacial Oxidation For Improving Visible Light Photocatalytic Hydrogen Evolution. *Appl. Catal., B* **2018**, *232*, 384.
(35) Wang, S.; Cao, J.; Cui, W.; Fan, L.; Li, X.; Li, D. Oxygen Vacancies and Grain Boundaries Potential Barriers Modulation Facilitated Formaldehyde Gas Sensing Performances for In2O3 Hierarchical Architectures. *Sens. Actuators, B* **2018**, *255*, 159.
(36) Arshavsky-Graham, S.; Massad-Ivanir, N.; Segal, E.; Weiss, S. Porous Silicon-Based Photonic Biosensors: Current Status and Emerging Applications. *Anal. Chem.* **2018**, *91*, 441.
(37) Choi, K.-S.; Chang, S.-P. Effect of Structure Morphologies on Hydrogen Gas Sensing by ZnO Nanotubes. *Mater. Lett.* **2018**, *230*, 48.
(38) Hejazi, S. M. H.; Aghazadeh Mohandesi, J.; Javanbakht, M. The Effect of Functionally Graded Porous Nano Structure TiO2 Photoanode on Efficiency of Dye Sensitized Solar Cells. *Sol. Energy* **2017**, *144*, 699.
(39) Seo, S.-J.; Hwang, Y. H.; Bae, B.-S. Post annealing Process for Low Temperature Processed Sol−Gel Zinc Tin Oxide Thin Film Transistors. *Electrochem. Solid-State Lett.* **2010**, *13*, H357.
(40) Di Valentin, C.; PAcchioni, G.; Selloni, A. Theory of Carbon Doping of Titanium Dioxide. *Chem. Mater.* **2005**, *17*, 6656.
(41) Sallis, S.; Quackenbush, N. F.; Williams, D. S.; Senger, M.; Woicik, J. C.; White, B. E.; Piper, L. F. J. Deep Subgap Feature in Amorphous Indium Gallium Zinc Oxide: Evidence Against Reduced Indium. *Phys. Status Solidi A* **2015**, *212*, 1471.
(42) Pachoumi, O.; Bakulin, A. A.; Sadhanala, A.; Sirringhaus, H.; Friend, R. H.; Vaynzof, Y. Improved Performance of ZnO/Polymer Hybrid Photovoltaic Devices by Combining Metal Oxide Doping and Interfacial Modification. *J. Phys. Chem. C* **2014**, *118*, 18945.
(43) Klein, A.; Körber, C.; Wachau, A.; Säuberlich, F.; Gassenbauer, Y.; Harvey, S. P.; Proffit, D. E.; Mason, T. O. Transparent Conducting Oxides for Photovoltaics: Manipulation of Fermi Level, Work Function and Energy Band Alignment. *Materials* **2010**, *3*, 4892.

https://doi.org/10.1021/acsami.1c09012
ACS Appl. Mater. Interfaces 2021, 13, 35981−35989